www.czasopisma.pan.pl PAN POLSKA AKADEMIA NAUK www.journals.pan.pl

Arch. Metall. Mater., Vol. 61 (2016), No 2, p. 657–664

DOI: 10.1515/amm-2016-0112

D. JUGOWIEC*, M. KOT**, T. MOSKALEWICZ*,#

ELECTROPHORETIC DEPOSITION AND CHARACTERISATION OF CHITOSAN COATINGS ON NEAR-β TITANIUM ALLOY

In this study, chitosan coatings were electrophoretically deposited (EPD) on near-β Ti-13Nb-13Zr alloy. The influence of colloidal solution composition and EPD parameters on the quality of chitosan coatings was investigated. It was established that the uniformity of as-deposited chitosan coatings is highly dependent on the chemical composition of the solution used for EPD, the pH, electrophoretic mobility and zeta potential of chitosan colloidal molecules, as well as EPD parameters, such as potential difference value and deposition time. The microstructure of the coatings was investigated using electron microscopy and X-ray diffractometry. The coatings 350 nm thick were homogeneous and exhibited an amorphous structure. The coatings had low hardness and Young's modulus. The effect of surface of the substrate preparation prior to coating deposition on the adhesion of chitosan coatings to the Ti-13Nb-13Zr alloy was also investigated. The coatings exhibited good adhesion to the non-acid-etched surface of the titanium alloy.

Keywords: chitosan, Ti-13Nb-13Zr alloy, electrophoretic deposition, coating

1. Introduction

Selecting materials for dental and orthopaedic implants in the biomedical field depends primarily on specific properties, such as excellent biocompatibility, adequate corrosion resistance and sufficient mechanical properties. The Young's modulus value of implants is required to be as close to those of human bone tissue as possible, in order to transfer the appropriate mechanical stress to the surrounding bone [1].

Titanium-based alloys have proven their capability as an implant material in bone surgery over many years in the field of oral implantology, osteosynthesis, and in certain applications in joint prosthetics [2]. This is mainly due to their excellent biocompatibility, good corrosion resistance, and chemical stability, as well as good tensile and fatigue strength, which results in a high strength to weight ratio [2-7]. In the last decade, two phase (α+β) Ti-6Al-4V and Ti-6Al-7Nb alloys have been extensively used as metallic implants in biomedical engineering. The main disadvantages of these particular alloys are the potentially harmful influence of their components (V, Al) on the human body and the relatively high elastic modulus value (approximately 110 GPa) [8]. Therefore, recent biomaterial research has focused on β titanium alloys, which provide enhanced properties, such as lower Young's modulus (approx. 30%), better ductility and increased corrosion resistance compared with α+β titanium alloys [2, 9]. However, implant-associated infections are still one of the most important complications of titanium implants, which ultimately lead to their failure [10]. The biocompatibility and antibacterial properties can be enhanced by surface modifications, either by adjusting the topography [11,12] or deposition of coatings with biocompatible and antibacterial components [13-15].

In the last decade, polymer coatings with antibacterial activities have attracted great interest in the biomedical field due to their ability to reduce implant-associated infections [16]. Chitosan, in particular, is one of the most promising natural biopolymers for tissue engineering [17]. This polysaccharide exhibits unique properties, such as antimicrobial activity, chemical stability and biocompatibility. Chitosan has been shown to be a versatile non-toxic material with a dual effect: it controls pathogenic microorganisms and activates several defence responses, inducing and/or inhibiting different biochemical activities during the organism-pathogen interaction. The positive charge of chitosan confers numerous and unique physiological and biological properties with great potential to this polymer, not only in the biomedical field, but also in pharmacology, cosmetology, biotechnology, food and agriculture [18-21].

Among different methods exploited for the production of biocompatible coatings, electrophoretic deposition (EPD) is particularly attractive due to its ability to produce uniform coatings with controlled properties on complex-shaped and porous structures at room temperature, as well as its low cost [22-23]. Moreover, it enjoys the advantages of fast deposition rate, high suspension stability and high production efficiency [24]. It is a process in which charged particles dispersed in a colloidal solution or suspension are moved and deposited onto oppositely charged electrodes

* AGH UNIVERSITY OF SCIENCE AND TECHNOLOGY, FACULTY OF METALS ENGINEERING AND INDUSTRIAL COMPUTER SCIENCE, 66 CZARNOWIEJSKA STR., 30-054 KRAKÓW, POLAND

** AGH UNIVERSITY OF SCIENCE AND TECHNOLOGY, FACULTY OF MECHANICAL ENGINEERING AND ROBOTICS, AL. MICKIEWICZA 30, 30-059 KRAKÓW, POLAND

Corresponding author: tmoskale@agh.edu.pl

under an electric field [25, 26]. The uniformity of the coating is very important for the development of high-quality implants. Most recent scientific works regarding EPD have focused on the factors influencing the coating quality, such as current intensity and suspension composition [27]. The thickness, morphology and hydrophobicity of the coatings can be significantly controlled by the applied electric field alone during EPD.

Numerous papers have been published concerning the electrophoretic deposition of chitosan coatings on stainless steel substrates [13, 28, 29]. Most of the papers present investigation of the kinetics of EPD of chitosan from aqueous dilute suspensions [13] and investigation of corrosion resistance of the coated steel [28]. But the substrate preparation prior EPD and investigation its influence on coatings adhesion is not sufficiently described in the literature. Therefore, the reference to the influence of substrate preparation prior to EPD on the adhesion of as-deposited chitosan coatings to the titanium alloy, is of great importance.

There is no information about the EPD of chitosan coatings on the Ti-13Nb-13Zr alloy, except for Łosiewicz et al. [30]. This investigation in particular shows an attempt to electrophoretically deposit a chitosan coating on the Ti-13Nb-13Zr alloy in an aqueous chitosan solution with acetic acid. There was a recurring problem with the deposition of homogeneous chitosan coatings due to the intensive formation of H_2 bubbles during water electrolysis. The novelty of the present work in comparison to Ref. [30] lies in the changing of the chemical composition of the aqueous chitosan solution with acetic acid by adding ethanol, in order to inhibit the hydrogen evolution process during electrolysis, and subsequently improve the uniformity of the chitosan coatings. The very important is also investigation of the effect of substrate preparation prior to EPD on the adhesion of chitosan coatings to the Ti-13Nb-13Zr alloy.

The aim of this work was to undertake a detailed investigation of suspension composition and EPD parameters (potential difference, deposition time) for the deposition of a uniform, good-quality chitosan coatings on near-β Ti-13Nb-13Zr alloy, as well as coatings microstructure and the influence of the substrate surface preparation prior EPD on coating adhesion.

2. Material and methods

A near-β Ti-13Nb-13Zr titanium alloy (13.5-13.7 Nb, 13.5-13.8 Zr, 0.05-0.06 Fe, 0.04 C, 0.01-0.02 N, 0.001 H, 0.11 O; wt %) delivered by Xi'an Saite Metal Materials Development Co., Ltd, China was used as a substrate for the EPD of chitosan coatings. Samples were in the shape of discs with a diameter of 27 mm and thickness of 2 mm. All of the samples were ground, polished and washed with ethanol prior to EPD. In addition, some of the specimens were immersed in 20% of HNO_3 for 10 minutes in order to remove the oxide layer from the substrate. A diluted solution of medium molecular weight chitosan (Sigma-Aldrich, Poland) (0.5 g/l) with a degree of deacetylation of about 75-85% in a mixture of distilled water and 1 vol. % acetic acid, as well as 9 diluted solutions of different concentrations of chitosan (0.5 g/l, 1 g/l, 2 g/l) in a mixture of distilled water, 50 vol. % ethanol and different vol. % of acetic acid (0.5%, 1% and 2%), were prepared by magnetic stirring at 300 rpm at room temperature for 24 hours and 72 hours and later used for EPD. The counter electrode was an AISI 316L austenitic stainless steel plate. EPD was carried out in a two-electrode cell, under constant voltage conditions in the range of 8-30 V. Deposition time was 4 minutes and the distance between electrodes in the EPD cells was 10 mm. The influence of the applied voltage, deposition time and chemical composition of the solution on current density during EPD have been investigated using a Tektronix DMM 4040 multimeter (USA). The zeta potential and electrophoretic mobility of the colloidal solutions were measured using a Zetasizer Nano ZS90 of Malvern Instruments Ltd., UK. PH values were measured using a Mettler Toledo EL20 pH-meter, China. The coating quality was evaluated by visual inspection and scanning electron microscopy (SEM) observations.

The microstructure of the Ti-13Nb-13Zr substrate and chitosan coatings were characterised by light microscopy (LM), SEM and transmission electron microscopy (TEM). The SEM investigation was carried out using an FEI Nova NanoSEM 450 (the Netherlands) and a Zeiss Neon Cross Beam 40EsB microscope (Germany). The TEM investigation was carried out using a JEOL JEM-2010 ARP microscope (Japan). Phase identification was performed by means of selected area electron diffraction (SAED) and by X-ray diffractometry (XRD). The XRD (Bragg-Brentano, B-B) and grazing incidence X-ray diffractometry (GIXRD) patterns were recorded using a Panalytical Empyrean DY1061 diffractometer (the Netherlands) applying Cu-Kα radiation and plan-view specimens. The cross-section lamella for the TEM investigation was prepared by a focus ion beam (FIB) using an FEI QUANTA 3D 200i device (the Netherlands). The chemical composition was analysed by energy dispersive X-ray spectroscopy (SEM-EDS). The micro-hardness and Young's modulus of the alloy were investigated by a Micro-Combi-Tester (MCT) device (CSM Instruments, Switzerland) with a Vickers indenter and load value of 1 N. The coating nanohardness and Young's modulus were measured by an NHT 50-183 of CSM Instruments. The adhesion of coatings to the substrate was analysed by a micro-scratch test using the MCT. The micro-scratch tests were performed using a Rockwell C indenter with a diamond tip radius of 200 μm, speed (dx/dt) of 5 mm/min, and load range of 0.03-10 N. The scratch length was 5 mm. The critical loads Lc1 and Lc2 (cohesive and adhesive cracks, respectively) were determined from LM observations, acoustic emission and friction force signals.

3. Results and discussion

3.1. Microstructure of the Ti-13Nb-13Zr alloy

Based on LM, SEM and TEM investigation, the Ti-13Nb-13Zr alloy exhibits a fine acicular martensite morphology. A typical image of the microstructure of the Ti-13Nb-13Zr

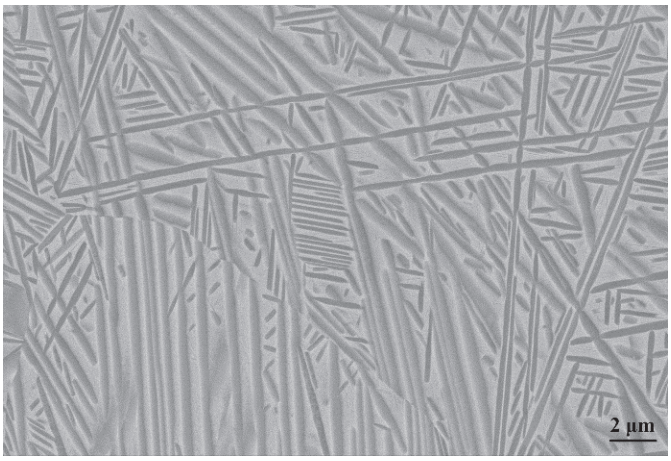

Fig. 1. Microstructure of the Ti-13Nb-13Zr alloy; SEM backscattered electron image (dark phase – α' laths, bright phase - β grains)

alloy observed by SEM is shown in Figure 1. The phase identification of the Ti-13Nb-13Zr alloy was performed by XRD (Fig. 2) and SAED (Fig. 3). The XRD and TEM investigation exhibited that the microstructure of the alloy was composed mainly of α' (hexagonal close-packed; hcp) laths in β (body-centered cubic; bcc) grains. Sporadically, fine α'' laths (orthorhombic, Cmcm space group) could also be observed. The grain size of the β phase ranged from 20 µm to 80 µm. The width of α' laths was up to 0.5 µm. The width of α'' laths was in the range of 5 nm to 25 nm. The mean chemical composition of the alloy investigated by SEM-EDS microanalysis was (in wt %): 74.6 Ti, 13.4 Zr and 12 Nb. STEM-EDS line analysis revealed an enrichment of Ti in the α' phase and Nb in the β phase (Fig. 4). The hardness and Young's modulus of the alloy were measured as 3 ± 0.2 GPa and 89 ± 2 GPa, respectively.

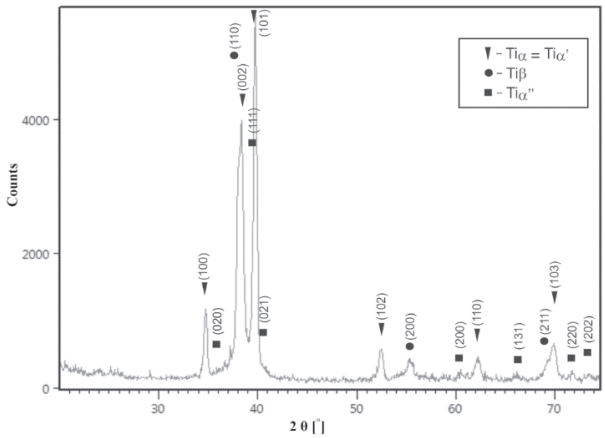

Fig. 2. XRD (B-B) pattern of the Ti-13Nb-13Zr alloy

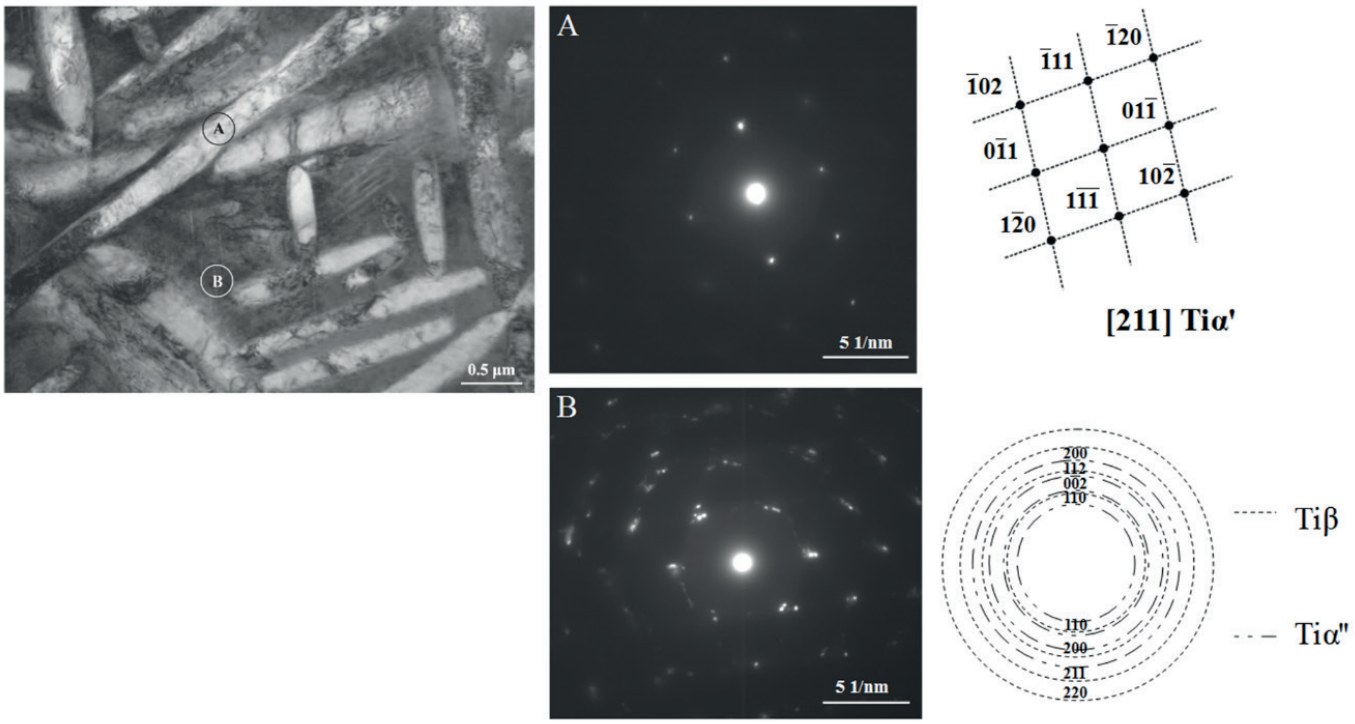

Fig. 3. Microstructure of the Ti-13Nb-13Zr alloy and SAED patterns taken from areas of α'phase (marked as A) as well as area of β and α'' phases (marked as B), TEM. The most intensive rings are marked for pattern B

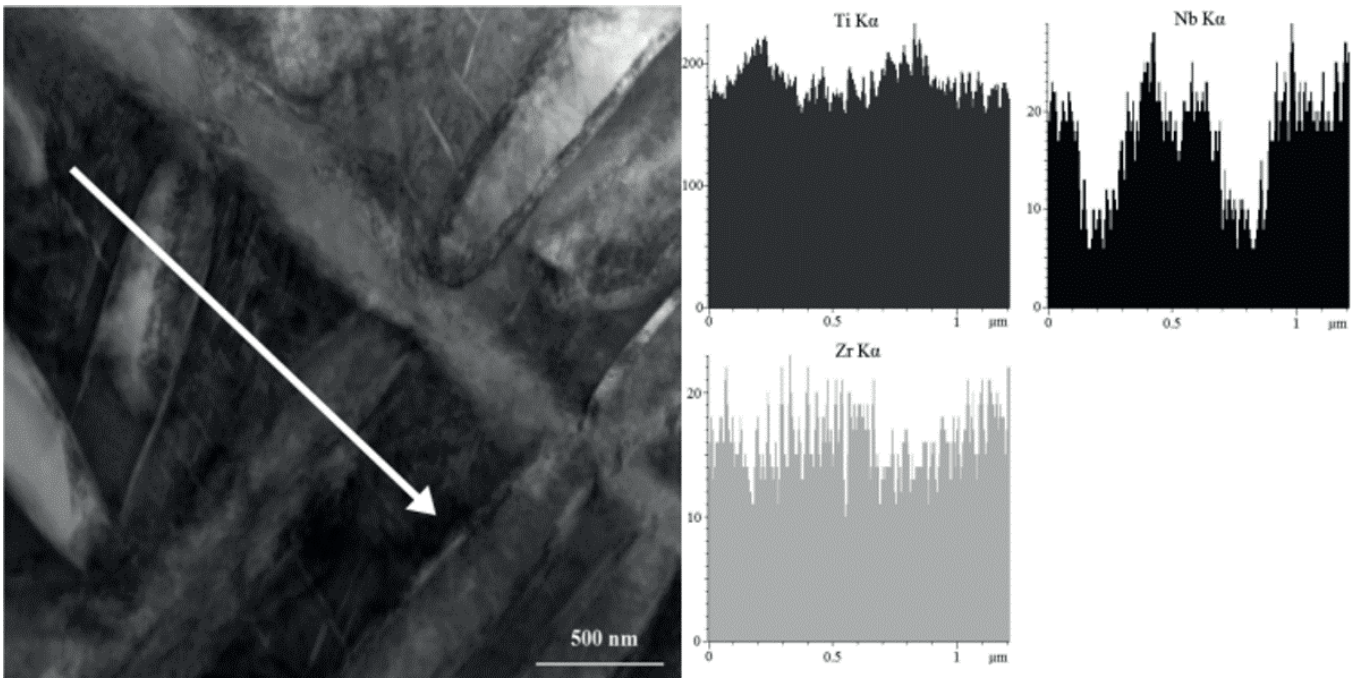

Fig. 4. STEM-BF micrograph of the Ti-13Nb-13Zr alloy microstructure and results of STEM-EDS linescan analysis of Ti, Zr and Nb performed along the line marked in the micrograph. The zero of the distance scale refers to the beginning of the arrow in the micrograph

3.2. Optimisation of suspension composition and EPD parameters for chitosan coating deposition

The electrophoretic mobility of suspended molecules in the solution is one of the main driving forces of EPD, and significantly affects the uniformity of as-deposited coatings. In our work, one diluted solution of chitosan in a mixture of acetic acid and distilled water, as well as nine different colloidal solutions of chitosan in a mixture of ethanol, acetic acid and distilled water, had their zeta potential and electrophoretic mobility investigated. The highest electrophoretic mobility (4.81 ± 0.64 cm·μm/Vs) was achieved for the solution of chitosan (1 g/l) in a mixture of distilled water and 1 vol. % of acetic acid (Fig. 5a,b). This can be correlated with its significantly lower viscosity compared with the other analysed chitosan solutions. The highest value of zeta potential (74.3 ± 3.8 mV) and the second highest value of electrophoretic mobility (2.5 ± 0.1 cm·μm/Vs) was achieved for the solution of chitosan (2 g/l) in a mixture of distilled water and 0.5 vol. % of acetic acid as well as 50 vol. % of ethanol. This solution also exhibited the highest pH value, equal to 4.4. It was found that chitosan molecules were positively charged under an electric field. Therefore a cathodophoresis approach during EPD was possible.

It was established that the pH value of chitosan solutions has a great influence on zeta potential and electrophoretic mobility values, but no direct relationship was found. Other parameters, such as chitosan content in the solution, also proved to greatly affect the electrophoretic mobility and zeta potential of the solutions. An increase in the chitosan content in the colloidal solution generally led to an increase in the pH value, zeta potential and electrophoretic mobility of the solution, simultaneously. It was also observed that an increase in water content in the colloidal solution leads to a formation of H_2 bubbles during EPD. This process was significantly intensive for the aqueous chitosan solution with 1 vol. % of acetic acid for the EPD of the chitosan coating. The presence of large H_2 bubbles significantly deteriorates the uniformity of the as-deposited coatings. A similar problem was reported in other investigations on the EPD of chitosan and chitosan/HA coatings, as described previously [29-34]. In the present work, a significant reduction in the formation of bubbles and thus better homogeneity of the coatings was obtained by using a solution of chitosan (0.5 g/l) in a mixture of distilled water and 1 vol. % of acetic acid as well as 50 vol. % of ethanol. The electrophoretic voltage value during EPD had a similar effect on the formation of H_2 bubbles. If the voltage was higher than 10 V, the formation of H_2 bubbles was very intensive. On the other hand, if the voltage value was lower than 10 V, the coating was only partially deposited on the substrate surface. The formation of H_2 bubbles might be explained by hydrogen evolution during the electrolysis of water under the influence of an electric field.

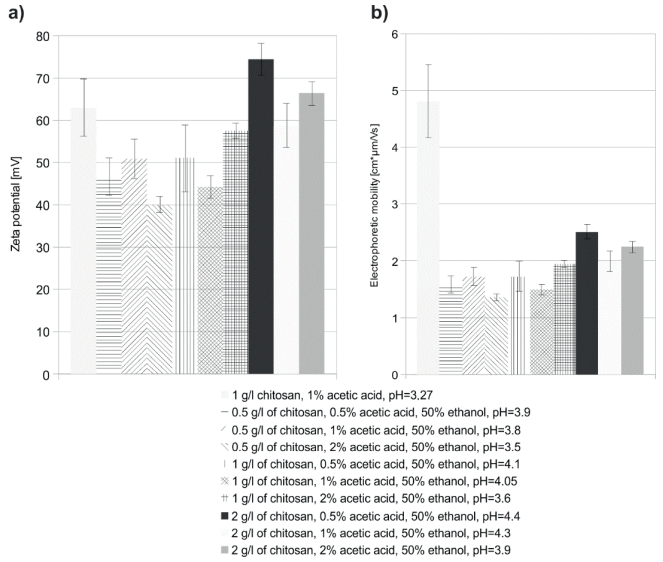

Fig. 5. Zeta potential (a) and electrophoretic mobility (b) for different composition of colloidal solutions used for EPD

During EPD, voltage and deposition time were determined in order to obtain homogeneous coatings. The most homogeneous and continuous coatings were deposited at the constant voltage of 10 V and deposition time of 4 minutes (Fig. 6). The direct relation between coating mass ingrowth and EPD parameters, such as set voltage value and deposition time, was also analysed. The weight gain was observed to be almost linear as a function of deposition time (Fig. 7a). The deposition weight increase as a function of voltage was nearly exponential (Fig. 7b). The increase in the voltage and deposition time led to higher coating mass ingrowth, but subsequently lower coating homogeneity. It was found that the current density value during EPD was very stable and its change pattern was similar for all nine different analysed solution compositions. The typical behaviour of current density as a function of deposition time is shown in Figures 8a,b.

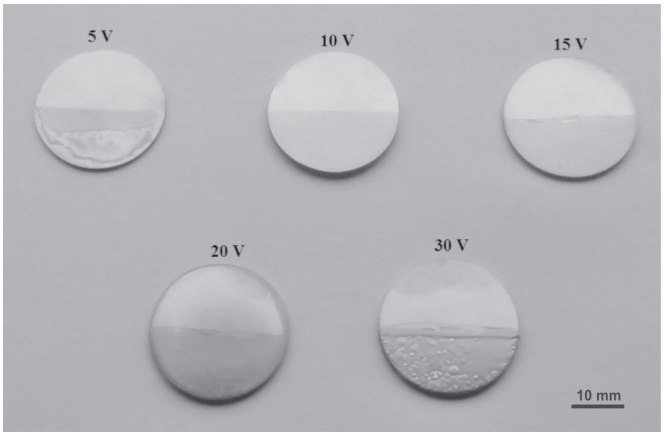

Fig. 6. Ti-13Nb-13Zr samples with chitosan coating deposited with set voltage values in the range of 5-30 V and constant deposition time of 4 minutes

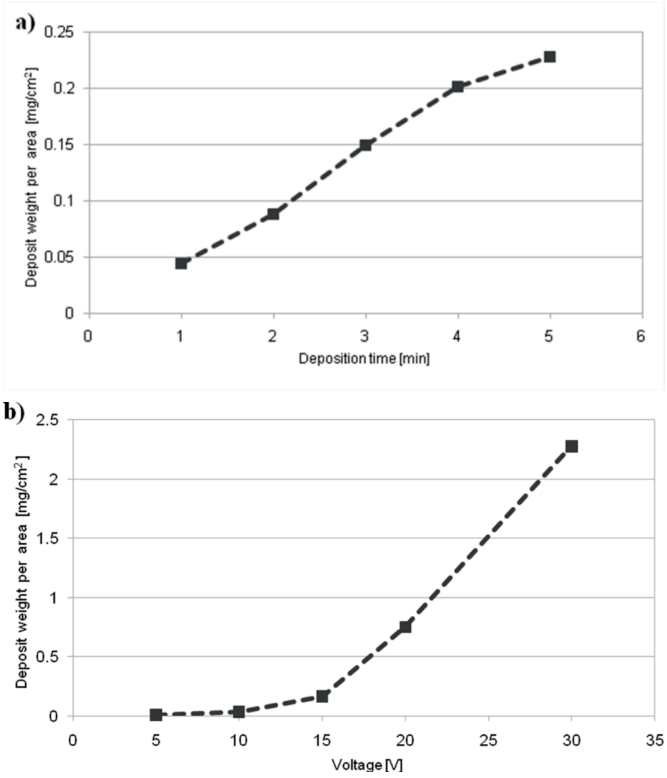

Fig. 7. Weight increase of as-deposited coatings for different deposition times and constant potential difference value of 10 V (a) as well as for different applied potential difference values and constant deposition time of 4 minutes (b)

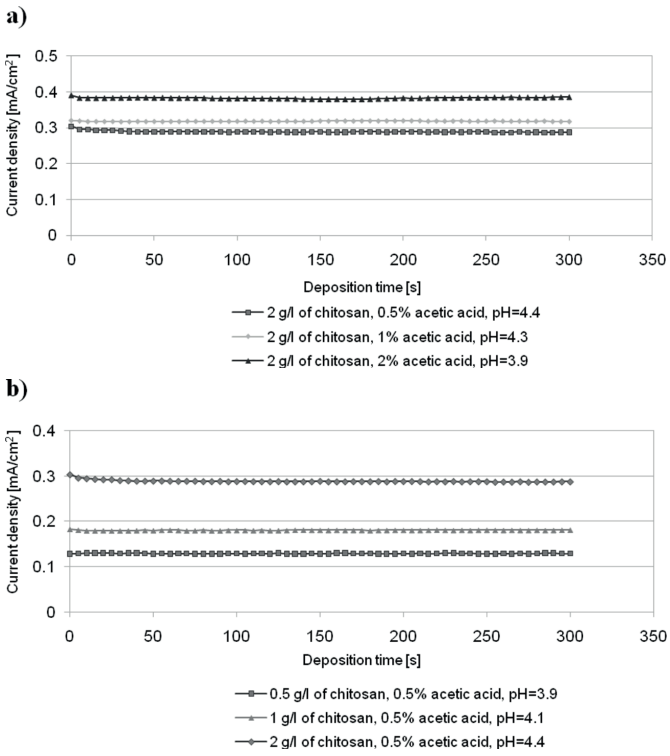

Fig. 8. Effect of deposition time on current density during EPD for different acetic acid concentration (a) and for different chitosan concentration (b) of colloidal solution

The mechanism for the EPD of chitosan was described in detail in Refs [14, 33-35]. According to these authors, positively charged chitosan molecules are prepared by protonation in the acetic acid solution and form cationic electrolytes, according to the following equation:

$$Chit - NH_2 - H_3O^+ \rightarrow Chit - NH_3^+ + H_2O \quad (1)$$

The absorption of chitosan on a negatively charged cathode is the result of chitosan macromolecule electrophoretic motion during EPD. The reaction at the cathode:

$$2H_2O + 2e^- \rightarrow H_2 + 2OH^- \quad (2)$$

leads to an increase in pH at the electrode surface and subsequently neutralization of the positively charged chitosan particles:

$$Chit - NH_3^+ + OH^- \rightarrow Chit - NH_2 + H_2O \quad (3)$$

Finally, the chitosan coating is deposited on the cathode (substrate) in the EPD cell.

SEM investigation of chitosan coating microstructure in the present work has shown that the duration of colloidal solution stirring before EPD has a significant influence on agglomerate formation and the overall homogeneity of chitosan coatings on near-β titanium alloy. The microstructure of chitosan coatings deposited in our work from a solution stirred only for 24 hours was full of chitosan agglomerates, which were unsuspended chitosan particles (Fig. 9a). On the other hand, the microstructure of chitosan coatings deposited from a solution stirred for 72 hours exhibited great uniformity and was free of any agglomerates (Fig. 9b). These findings have also been confirmed by AFM investigation. Typical images of surface topography of the coatings deposited from a solution stirred for 24 hours and 72 hours are shown in Figures 10a,b. Chitosan particles are clearly visible in Figure 10a, while the coating in Figure 10b is free of chitosan particles.

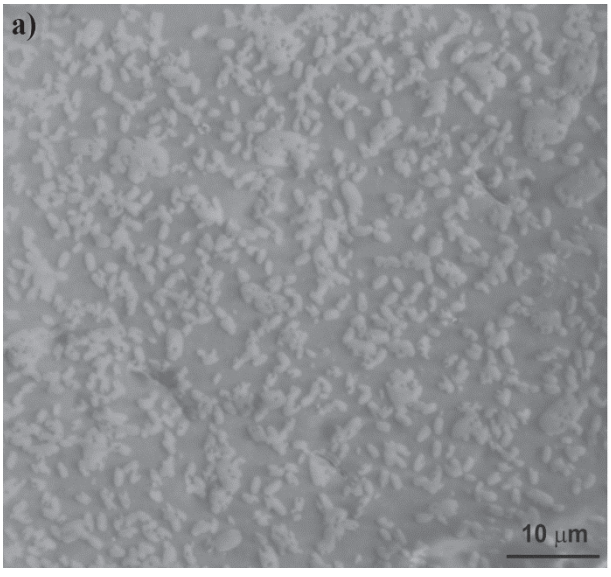

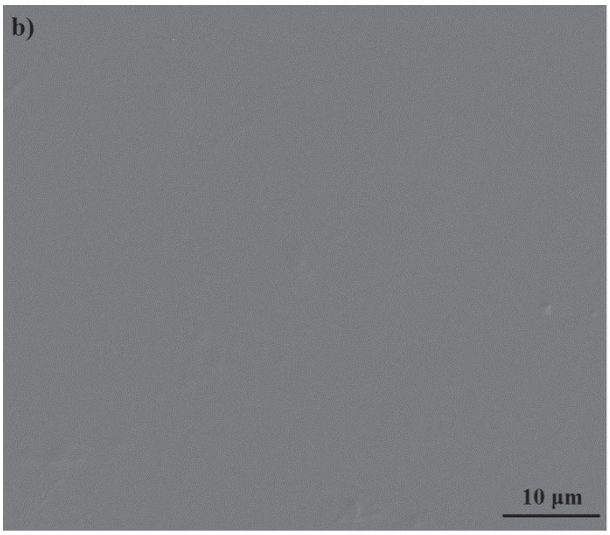

Fig. 9. Microstructure of chitosan coatings on near-β Ti-13Nb-13Zr alloy deposited from solution of chitosan (2 g/l) in a mixture of distilled water and 0.5 vol. % of acetic acid as well as 50 vol. % of ethanol stirred for 24 hours (a) and 72 hours (b), SEM plan-view specimens

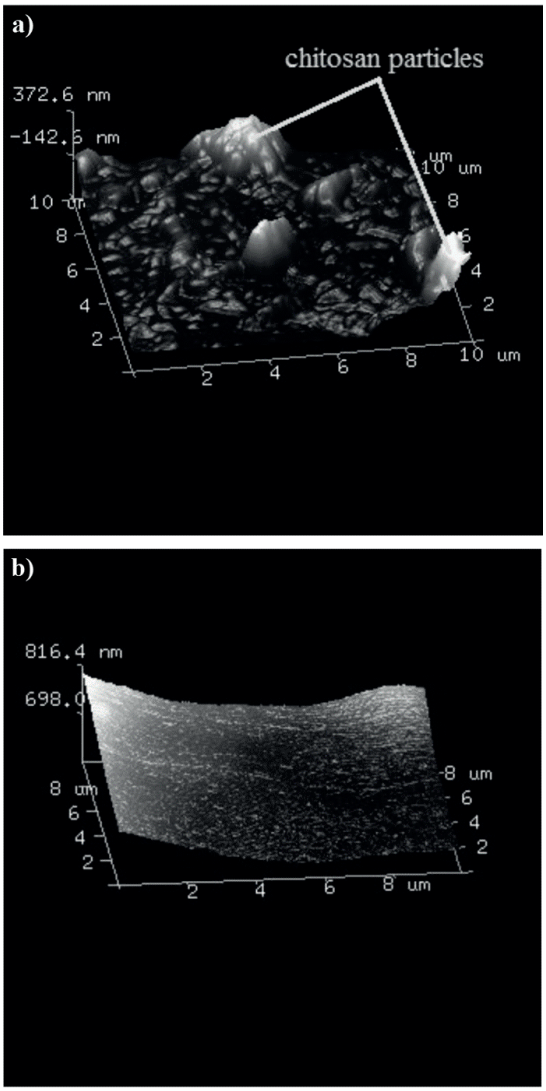

Fig. 10. Surface topography of chitosan coating on near-β Ti-13Nb-13Zr alloy deposited from solution of chitosan (2 g/l) in a mixture of distilled water and 0.5 vol. % of acetic acid as well as 50 vol. % of ethanol stirred for 24 hours (a) and 72 hours (b), AFM

3.3. Microstructure and properties of chitosan coatings on the Ti-13Nb-13Zr alloy

Microstructure and properties investigation was performed for the best quality coating deposited from a solution of chitosan (2 g/l) in a mixture of distilled water and 0.5 vol. % of acetic acid as well as 50 vol. % of ethanol stirred for 72 hours. SEM observations revealed that the chitosan coating was continuous and homogeneous. The coating thickness was measured on TEM images (Fig. 11) as about 350 nm. SAED pattern analysis revealed the occurrence of an amorphous phase in the coating.

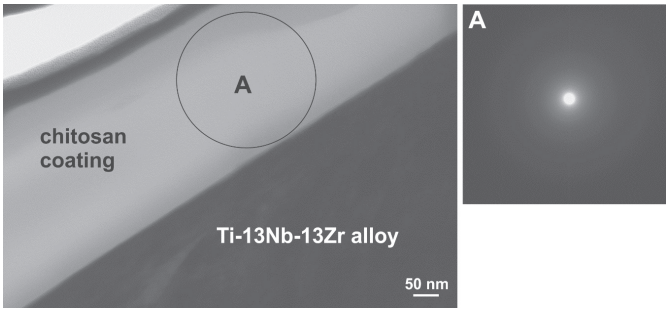

Fig. 11. Microstructure of the chitosan coating on Ti-13Nb-13Zr alloy and SAED pattern taken from coating area marked as A, TEM, FIB lamella

Grazing incidence X-ray diffraction was applied for the investigation of a thin chitosan coating. A broad peak was observed in the GIXRD spectrum at approx. 2θ, equal to 15-20º, which confirmed the presence of amorphous phase in the coating (Fig. 12). The strong peaks of substrate material in the spectrum also confirmed a very small coating thickness.

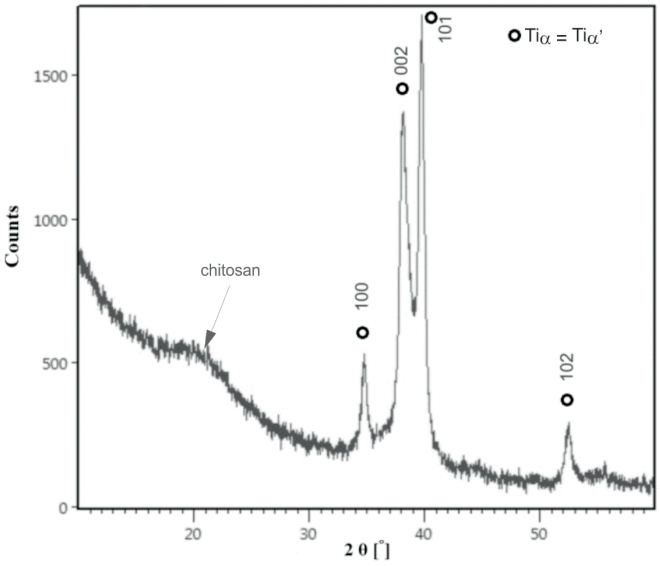

Fig. 12. GIXRD pattern of chitosan coating deposited at potential difference of 10 V during 4 minutes on Ti-13Nb-13Zr alloy. The pattern was performed at low incidence angle of 1º

Micro-scratch testing revealed relatively good adhesion of chitosan coatings to the non-acid-etched Ti-13Nb-13Zr alloy substrate, better than those of the acid-etched substrate. No cohesive cracks were observed in the coating. The measured critical load Lc_2 was 3.2 N. At this load, the first delamination of coatings appeared on the borders of scratch tracks. The increase in load up to 5 N resulted in the rapid intensification of this process and subsequent removal of large area chitosan coatings around scratches. The adhesion of the chitosan coating deposited on the acid-etched Ti-13Nb-13Zr substrate was lower than that of the one deposited on the non-acid-etched one. The measured critical load Lc2 in this case was 1 N and rose to 2 N, which led to the complete removal of chitosan coatings around scratches. It can be concluded that acid-etching of the Ti-13Nb-13Zr alloy surface deteriorates the chitosan adhesion to the substrate, due to removal of passive oxide layer. The nano-hardness and Young's modulus of the chitosan coating were measured on the plan-view specimen and ranged from 0.64 GPa to 1.08 GPa, as well as from 17 GPa to 30.3 GPa, respectively, for different penetration depth of the indenter (Fig. 13).

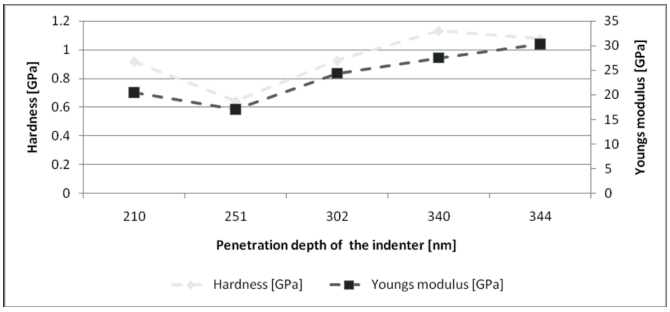

Fig. 13. Nanohardness and Young's modulus of the chitosan coating on Ti-13Nb-13Zr alloy measured for different penetration depths of the indenter

4. Conclusions

The EPD of chitosan coatings on near-β Ti-13Nb-13Zr titanium alloy was successful. The appropriate colloidal solution composition was selected based on measured zeta potential and electrophoretic mobility values as well as visual observation of the coated specimens. The highest values of electrophoretic mobility and zeta potential were achieved for the water based colloidal solution. However, the solution of chitosan (2 g/l) in a mixture of distilled water and 0.5 vol. % of acetic acid as well as 50 vol. % of ethanol, was used to coating deposition due to the better coating quality.

It was found that the uniformity of the as-deposited chitosan coating is highly dependent on the colloidal solution composition and stirring prior to EPD, as well as potential difference value and deposition time during EPD. The most homogeneous and continuous coatings were deposited at the constant potential difference of 10 V and deposition time of 4 minutes. The increase in potential difference values and deposition times led to higher coating mass ingrowth but subsequently lower homogeneity. The coatings were amorphous. A relatively good adhesion of chitosan coating to the non-acid-etched Ti-13Nb-13Zr alloy substrate was found during micro-scratch testing.

Acknowledgments

This work was supported by the Polish National Science Centre (decision no. DEC-2013/09/B/ST8/00145).

The authors appreciate a valuable contribution of Dr Ł. Cieniek, Dr A. Radziszewska and A. Gruszczyński, MSc (AGH-University of Science and Technology) to SEM and XRD investigation as well as Dr M. Gajewska (ACMIN) for FIB lamella preparation.

REFERENCES

[1] O. Floręncio, P.S. Silva Jr., R. Ribeiro, J.M. Chaves, F.H. Sá, F.X. Melo, S.G. Schneider, Mater. Sci. Eng. **A 521-522**, 351-353 (2009).
[2] E.B. Taddei, V.A.R. Henriques, C.R.M. Silva, C.A.A. Cairo, Mater. Sci. Eng. C **24**, 683-687 (2004).
[3] M. Sowa, M. Piotrowska, M. Widziołek, G. Dercz, G. Tylko, T. Gorewoda, A.M. Osyczka, W. Simka, Mater. Sci. Eng. C **49**, 159-173 (2015).
[4] P. Majumdar, S.B. Singh, S. Dhara, M. Chakraborty, Mater. Sci. Eng. C **46**, 62-68 (2015).
[5] L. Mohan, C. Anandan, Appl. Surf. Sci. **282**, 281-290 (2013).
[6] A. Zieliński, P. Antoniuk, K. Krzysztofowicz, Surf. Eng. **30**, 643-649 (2014).
[7] S.J. Wu, H. Li, S.Y. Wu, Q. Guo, B. Guo, Surf. Eng. **30**, 693-696 (2014).
[8] W. Simka, R.P. Soch, G. Dercz, J. Michalska, A. Maciej, A. Krząkała, Appl. Surf. Sci. **279**, 317-323 (2013).
[9] C.A.R.P. Baptista, S.G. Schneider, E.B. Taddei, H.M. da Silva, Int. J. Fatique **26**, 967-973 (2004).
[10] F. Ordikhani, A. Simchi, Appl. Surf. Sci. **317**, 56-66 (2014).
[11] X. Liu, P.K. Chu, C. Ding, Mater. Sci. Eng. R **47**, 49-121 (2004).
[12] M.T. Mohammed, Z.A. Khan, A.N. Siddiquee, Procedia Mater. Sci. **6**, 1610-1618 (2014).
[13] A. Simchi, F. Pishbin , A.R. Boccaccini, Mater. Lett. **63**, 2253-2256 (2009).
[14] Y. Li, X. Pang, R.F. Epand, I. Zhitomirsky, Mater. Lett. **65**, 1463-1465 (2011).
[15] Y. Cheng, K. M. Gray, L. David, I. Royaud, G. F. Payne and G. W. Rubloff, Mater. Lett. **87**, 97-100 (2012).
[16] F. Ding, Z. Nie, H. Deng, L. Xiao, Y. Du, X. Shi, Carbohydr. Polym. **98**, 1547-1552 (2013).
[17] X. Pang, T. Casagrande, I. Zhitomirsky, J. Colloid Interface Sci. **330**, 323-329 (2009).
[18] X. Cheng, K. Ma, R. Li, X. Ren, T. S. Huang, Appl. Surf. Sci. **309**, 138-143 (2014).
[19] M. Z. Elsabee , E. S. Abdou, Mater. Sci. Eng. C **33**, 1819-1841 (2013).
[20] G. Ruhi, O.P. Modi, S.K. Dhawan, Synth. Met. **200**, 24-39 (2015).
[21] S. Bautista-Baños, A.N. Hernández-Lauzardo, M.G. Velázquez-del Valle, M. Hernández-López, E. Ait Barka, E. Bosquez-Molina, C.L. Wilson, Crop Prot. **25**, 108-118 (2006).
[22] F. Pishbin, V. Mouriño, J.B. Gilchrist, D.W. McComb, S. Kreppel, V. Salih, M. P. Ryan, A. R. Boccaccini, Acta Biomater. **9**, 7469-7479 (2013).
[23] J. Lou, K. Yu, G. Wei, C. Xin, Y. Qin, L. Jiang, H. Ge, H. Dettinger, Surf. Eng. **29**, 637-641 (2013).
[24] Y. Wang, M. Kang, S.W. Jin, X .Q. Fu , X. S. Wang, Surf. Eng. **30**, 557-561 (2014).
[25] Z. Wang, X. Zhang, J. Gu, H. Yang, J. Nie , G. Ma, Carbohydr. Polym. **103**, 38-45 (2014).
[26] I. Corni, M. P. Ryan and A. R. Boccaccini, J. Eur. Ceram. Soc. **28**, 1353-1367 (2008).
[27] Z. Zhang, X. Wu, C. Jiang , N. Ma, Surf. Eng. **30**, 21-25 (2014).
[28] F. Gebhardt, S. Seuss, M.C. Turhan, H. Hornberger, S. Virtanen, A. R. Boccaccini, Mater. Lett. **66**, 302-304 (2012).
[29] I. Zhitomirsky ,d A. Hashambhoy, J. Mater. Process. Technol. **191**, 68-72 (2007).
[30] B. Łosiewicz, G. Dercz, M. Szklarska, W. Simka, M. Łężniak, A. Krząkała , A. Swinarew, Solid State Phenom. **203-204**, 212-215 (2013).
[31] L. Altomare, L. Draghi, R. Chiesa, L. De Nardo, Mater. Lett. **78**, 18-21 (2012).
[32] T. Moskalewicz, M. Kot, S. Seuss, A. Kędzierska, A. Czyrska-Filemonowicz, A. Boccaccini, Met. Mater. Int. **21**, 96-103 (2015).
[33] J. Zhang, Z. Wen, M. Zhao, G. Li , C. Dai, Mater. Sci. Eng. C 58, 992-1000 (2016).
[34] X. Pang and I. Zhitomirsky, Mater. Charact. **58**, 339-348 (2007).
[35] S. Mahmoodi, L. Sorkhi, M. Farrokhi-Rad, T. Shahrabi, Surf. Coat. Technol. **216**, 106-114 (2013).